Dry and Wet Periods in the Northwestern Maghreb for Present Day and Future Climate Conditions

K. Born[(1)], A. H. Fink[(1)] and H. Paeth[(2)]

(1) Institute for Geophysics and Meteorology, University Cologne, Germany.

(2) Institute for Geography, University Würzburg, Germany.

Contact

Dr. Kai Born (corresponding author)
Institut für Geophysik und Meteorologie der Universität zu Köln
Kerpener Str. 13
50937 Köln
e-mail: kai.born@uni-koeln.de
Tel.: +49 221 4703686

Dr. habil. Andreas H. Fink
Institut für Geophysik und Meteorologie der Universität zu Köln
Kerpener Str. 13
50937 Köln
e-mail: andreas.fink@uni-koeln.de
Tel.: +49 221 4703819

Prof. Dr. Heiko Paeth
Institut für Geographie
Am Hubland
97074 Würzburg
e-mail: heiko.paeth@uni-wuerzburg.de
Tel.: +49 931 8884688

Abstract

One urgent issue of climate research is the regional downscaling of global-scale climate scenarios. The present study, which is part of the research of the IMPETUS West-Africa project, shows an analysis of wet and dry periods in north-western Africa both from observed rainfall and from scenarios obtained from an ensemble study of the regional climate model REMO. One question is how different sources of data with different quality and different statistical characteristics can be interpreted with respect to the future development of rainfall variability. The Köppen climate classification of the very heterogeneous investigation area reveals a bias of the regional model climate scenarios towards dryer conditions. Three regions of similar rainfall variability are marked by a principal component analysis of rainfall data. For these three regions, homogenization is achieved by calculation of standardized precipitation indices (SPI). The SPI series are evaluated with respect to return times of sufficiently high/low values. For this purpose, an extreme value analysis using a fit of the generalized Pareto distribution (GPD) is compared with return values from empirical rainfall distributions. Despite the model bias, both analysis methods reveal a persistence and intensification of the observed climate shift towards shorter return times of stronger dry periods in climate scenarios under greenhouse gas forcing.

1. Introduction

Morocco is located between the arid regions of the western Sahara and the moderate Mediterranean and Atlantic regions. The arid regions are marked by weak seasonal variations with episodic rainfall, whereas in the Mediterranean and Atlantic regions moderate, wet winters and hot, dry summers prevail (Griffiths, 1972; Griffiths and Soliman, 1972). Landscape types cover agricultural areas with seasonal varying productivity and vegetation canopy in a flat or moderately hilly environment in the north-western part, high mountain areas in the Atlas and Rif regions and semi-desert shrub land, grassland and desert in the southern part. In these climatic zones, agricultural production and local economy depend very much on water availability, and thus, is expected to be subject to the impact of ongoing and future climate changes. In the past, periods of successive dry years have repeatedly shown the vulnerability to water scarcity, which results in threatened livelihoods of farmers and nomad families living from pasturing. In order to counteract the peril of water scarcity, regional planning greatly benefits from information on future climate variability. Of course, the provision of reliable future climate scenarios in this very heterogeneous region is still a challenge for the climate research community. In particular the regional characteristics of climate change cannot be derived from global climate model (or general circulation model, GCM) studies due to their coarse grid sizes. The necessary next step is a downscaling of global climate model scenarios to the region of interest. In this study, results of a dynamical downscaling of ECHAM GCM scenarios (Roeckner et al.,2003) using the regional climate model (RCM) REMO (Jacob et al., 2001) in 0.5°x0.5° lat.-lon. resolution are analyzed in order to asses possible climate change for the time up to the year 2050.

It should be mentioned that the term “drought” in general is understood in its socio-economic and agricultural context. Droughts have a lot of forcing factors and indicators which are not connected to weather or climate. Commonly used definitions of drought periods have subjective aspects and depend, among others, on economic conditions. From that point of view it is clear that drought

detection is not possible solely from atmospheric observations. This study, however, focuses simply on dry and wet periods which can easily be detected from rainfall observations, instead on a more complex definition of drought.

Among the studies on climate in Morocco, some historical attempts do not utilize only atmospheric observational data for climate classification. Comparable to Köppens climate classification (Köppen, 1936), Emberger (1930 and 1955) defined a biogeographical climate classification for the south-west Mediterranean and Morocco, by considering plant populations and the seasonal march of temperature and rainfall. Since the impact of climate variability and change on vegetation is one of the most important topics in climate change assessment, this approach may be quite useful for identifying regional climate patterns. But unfortunately, vegetation is also influenced by anthropogenic activities and thus, is no longer a clear indicator for climate conditions. Therefore, studies using a bioclimatic approach are extremely labour intensive in order to assess non-disturbed vegetation (see e. g. Finckh et al., 2007).

Recent studies mostly use the meteorological-climatological approach and concentrate on rainfall variability and atmospheric forcing. A general overview of observed rainfall variability in Africa is given in Nicholson (2000). Focussing on northwest Africa, the influence of teleconnection mechanisms like the North Atlantic Oscillation (NAO) or El Niño/Southern Oscillation (ENSO) on rainfall have been primarily investigated (Lamb and Peppler, 1987; Lamb et al., 1997; Portis et al., 2001). Ward et al (1999) analyze the climate of northern Africa with more meteorological methods and describe an interaction between Sahel droughts and rainfall variability north of the Sahara. The forcing of wintertime rainfall in north-western Africa has been examined in Knippertz (2004). The tropical-extratropical link has also been examined by Jung et al. (2006), but from the other point of view: The study focuses on the forcing of Sahelian rainfall by the extreme conditions in the Mediterranean in summer 2003. Seasonal predictability of rainfall in the Maghreb has been examined by El Hamly et al. (1998) using the NAO as predictor, which shows acceptable forecast skill only north of the Atlas Mountains.

The observational data used in the present study have been introduced in Knippertz et al. (2003), along with an analysis of larger scale weather conditions leading to wet and dry periods in Morocco. The NAO index is, at least for interannual and longer time scales, connected to northern Atlantic SST. Li et al. (2003) have studied statistical modes of Atlantic sea surface temperature (SST) and its influence on seasonal variations of rainfall in north-west Africa using NCEP/NCAR reanalysis data and results from the NCEP GCM in an ensemble of 100 runs, each of eight months duration. Existing studies which emphasize sophisticated statistical methods to characterize dry and wet periods focus on the Mediterranean region but not on the north-western Maghreb. An analysis of rainfall data from NCEP reanalysis in Europe which allows for an interpretation in the Mediterranean has been carried out by Bordi and Sutera (2001). The techniques used in that study are similar to the methods used here, but are applied on NCEP reanalysis data and focus more on the larger scale forcing of wet and dry

conditions by the flow pattern of the northern hemispheric atmosphere. An extreme value analysis in the Mediterranean area with respect to the impact of global warming on extreme values of daily rainfall is presented in Paeth and Hense (2005). In fact, Paeth and Hense (2005) analyzed data from a former RCM study using REMO (Paeth et al., 2005), which consisted of a present day climate model run from 1979 to 2003 and of time-slices for the future scenarios. This model data base did not allow for an investigation of the frequency and relevance of dry and wet periods. Thus, their study has been extended and now contains the ensemble of present-day and future climate scenarios used in the present study. A more detailed description of the model setup and results is given in Paeth et al., 2008. An example of dry and wet period analysis of observational data on a longer-term scale in the Mediterranean has been given by Bordi et al. (2006) for Sicily. That study demonstrates state-of-the-art statistical methods for the identification of extreme wet and dry conditions in a very heterogeneous environment.

A particular problem of research on future climate change is that data available for comparison are often not consistent. For present day conditions, direct observations and gridded data like reanalyses are used; from the outset these two sources have different characteristics. For future climate, climate models show a reasonable bias for present day conditions and have both physical and conceptual shortcomings, because they represent an approximation of the climate system. The problems become worse when looking on smaller scales. The question is now: Are we able to make reliable statements on regional patterns of future climate despite these problems? Although this question has been addressed quite often, there is no commonly used recipe to solve this problem. Among the variety of techniques used, we have chosen the idea to formulate a normalized index in order to omit both spatial and model-based heterogeneities.

In this study, the regional climate of the north-western Maghreb is analyzed from observations and from regional climate model data. The focus of the study is solely on rainfall, although temperature changes will also have an effect on future drought conditions. It consists of four chapters: First, data and methods are introduced briefly. In the second part, a general overview of present day and future climate conditions from regional climate modelling are presented. The Köppen climate classification is deployed in order to asses a possible impact on the vegetation. A principal component analysis (PCA) is applied on observed rainfall at stations in order to define regions of similar rainfall characteristics. In the third part, the recurrence of wet and dry years in observations and climate scenarios for three characteristic regions which were detected by the PCA is examined. For that purpose, an extreme value analysis is applied on time series of the standardized precipitation index (SPI) after McKee et al. (1993). Finally, a summary of the results is presented. Details of the used statistical methods are described in the Appendices.

2. Data and Methods

Observations

Analysis of climate and climate variability always starts with the acquisition of observational information in the region of interest. In Morocco, the density and quality of observations is better than in most other parts of northern Africa, but still relatively sparse compared to Europe. The first and most important source of information stems from SYNOP weather stations, which contribute to the WMO network and have delivered data of a relatively high quality standard for several decades now. The data set used in this study is part of the Global Historical Climatology Network (GHCN) and was originally provided by the Office of Climatology of the Arizona State University (Vose et al., 1992). The GHCN data has already been utilized in the same region by Knippertz et al. (2003) and has, for the present study, been extended to cover the period 1841-2007. For the present study, only monthly rainfall sums have been used. Unfortunately, most stations in Morocco and the western parts of Algeria are located north of the Atlas Mountains (see Fig. 1). This leaves a lack of information in the southern region, where the impact of a climate shift is expected to be very strong. In principle, the GHCN data can be extended by information from individual climate stations operated mainly by regional water management facilities, but the quality standard and temporal completeness of these data is not as high as for GHCN data. Therefore, we use only three additional climate stations located at the southern slope of the High Atlas Mountains in order to enhance the reliability of the assessment south of the Atlas at least a little bit. These additional stations are checked carefully and are able to improve the description of rainfall in the semi-arid region between the Atlas Mountains and the Sahara.

For climate classification, the rainfall data have to be accompanied by temperature observations. Thus, we also used the gridded version of historical climate data provided by the Climate Research Unit of the University of East Anglia, hereafter referred to as CRU TS2.1 (Mitchell and Jones, 2005). These data also contain near-surface temperature and cover the period 1901-2002. Their quality standard is very high, but precipitation is estimated for grid boxes using correlations between stations in order to conserve the statistical properties of the rainfall. As a consequence, we were not certain if rainfall variability from stations lying far away is able to distort the behaviour of our characteristic regions we define by the PCA. To omit this uncertainty we decided to take GHCN data for the PCA and CRU TS2.1 for climate classification and comparison with RCM data. The CRU TS2.1 has been supplemented with rainfall data from a data set obtained from the VASCLIMO (Variability Analysis of Surface Climate Observations) project (Beck et al., 2005).

RCM data

In order to assess future climate conditions, data of a RCM was used. The RCM study has been undertaken with the mesoscale atmospheric model REMO of the *Max-Planck Institute for Meteorology* (MPIfM) Hamburg. REMO is based on the hydrostatic approximated set of hydrodynamic equations. The package of physical parameterizations is similar to the one of the ECHAM5 GCM in order to produce consistent results when REMO is nested into ECHAM5. The

model area for this RCM application contains North Africa and the Mediterranean (15°S-45°N, 30°W-60°E). Further details of model physics are described in Jacob et al. (2001), the application of REMO for RCM studies in the Mediterranean and Africa has been presented in Paeth (2004), Paeth et al. (2005), and Paeth and Hense (2005). REMO has been applied in ensemble mode for the periods 1960-2000 (3 Control runs, C20) and for 2001-2050 (6 scenario runs, 3 x SRES A1B and 3 x SRES B1) in order to study the possible future development of climate in Northern Africa. The large-scale atmospheric forcing was provided by scenario runs of the ocean-atmosphere general circulation model (OAGCM) ECHAM5/MPI-OM (Roeckner et al., 2003), which participated in the 4th IPCC report (IPCC, 2007). The climate forcing in REMO consists of the anthropogenically enhanced greenhouse gas (GHG) effect and SST changes, mainly inferred from the GCM, as well as land cover changes (LCC), which were assessed on the basis of FAO (Food and Agriculture Organization of the United Nations) studies. LCC is limited to Sub-Saharan Africa and contains the impacts of deforestation, desertification and the transition of natural vegetation into arable lands. Details and results of the RCM study are presented in Paeth et al. (2008). It has to be kept in mind that the SST variability simulated by the OAGCM is not in phase with observed SST anomalies on shorter time scales. As a consequence, present day climate simulated with the OAGCM is not expected to coincide with observations of single years. Only the statistical characteristics of OAGCM simulations and observations on typical climatic scales should be reproduced.

Statistical methods

This article will not cover the whole spectrum of climatic aspects; instead we concentrate on rainfall variability. For the overview of climate in north-western Africa and of RCM performance, the Köppen climate classification (Köppen, 1936) is applied to observed and model data. Because rainfall is very heterogeneous in space and time, a preliminary principal component analysis (PCA) is performed in order to find regions in which rainfall observations are statistically connected. The PCA technique is very often used in climate research; originally it was introduced by Pearson (1901) and has been refined by Hotelling (1933). Preisendorfer (1988) gives a comprehensive overview on the PCA application. The PCA is briefly described in Appendix B.

The spatial heterogeneity of rainfall observations demands a standardization of rainfall data. One method, performed in the former study of Knippertz et al. (2003) is to calculate a quintile index (QI, WMO, 1983). Five equally spaced rainfall classes are defined from observed rainfall distributions in time. According to its value, each observation is located in one of the classes. The number of the class (1-5) is the QI. One disadvantage is that QI values are integer numbers and do not really permit an extreme value analysis. In order to overcome this disadvantage, in the present study the standardized precipitation index (SPI) following McKee et al. (1993) and Guttmann (1999) is used. The goal of formulating the SPI is to transform the usually heavily skewed probability density function (PDF) of rainfall data into a Gaussian normal distributed parameter. Large negative or positive values of the SPI

correspond with extreme dry and wet conditions, respectively. The calculations performed to obtain the SPI series is described in Appendix C. SPI values closely follow a Gaussian normal distribution, although still problems in regions with considerable amounts of zero values may occur.

The frequency of dry and wet periods is then analyzed with an extreme value analysis. In the simple approach return values are calculated directly from the empirical cumulative distribution (ECD) and from Gaussian kernel estimation. The tail of a distribution above/below a certain threshold is fitted by a Generalized Pareto Distribution (GPD). The GPD parameters are used to calculate return times and levels. Further details of statistical methods used here are described more detailed in Appendix D.

3. Present Day and Future Moroccan Climate: An Overview

Köppen climate classification

Climate variability affects vegetation in both natural and agricultural environments. Therefore, our first view focuses on the well-known Köppen climate classification, which is based on thresholds relevant for special vegetation types. We want to demonstrate the climate shift in the late 20th century by comparison of climate classes obtained from a reduced version of Köppens classification scheme, which has already proven its practicability in other applications (Guetter and Kutzbach, 1990, Fraedrich et al. 2001, Kottek et al., 2006). Using the same data, Fraedrich et al. (2001) have shown that the – in a statistical sense – optimal length of time spans for detecting changes in the Köppen classification is 15 years. Therefore, classification is applied to the 15-year periods 1951-65 and 1986-2000. Figure 2 shows the classification results for the entire Mediterranean basin; in Table 1 the climate classes are listed. In northern Africa we can clearly see a shift towards dryer and warmer climates; at the borders to Steppe and Desert a number of pixels shift from moderate and summer dry (*Cs*) to Steppe climates. The results are in accordance with the above-mentioned studies from Fraedrich et al. (2001) and Kottek et al. (2006). For future climate, Fig. 3 shows the same classification for the RCM data for the periods 1986-2000 and 2036-2050 of the SRES A1B scenario. First, the RCM bias can be seen clearly: in the south-western Atlantic region, model climate is shifted towards Steppe and desert climates (cf. Fig. 2, lower panel and Fig.3, upper panel). Since the climate system is highly complex, this existence of a bias is not astonishing. For assessment of the future climate change, only relative changes between present-day model climate and future model climate should be taken into account. The relative changes between 1986-2000 and 2036-2050 – also in other parts of northern Africa, which are not shown here – show a warming and drying trend similar to the observed changes in the 20th century, albeit a little stronger.

In summary, the REMO model reveals a continuing and strengthening climate change towards dryer and warmer conditions all over Morocco. The warming is in accordance both with 20th century observations and with global temperature changes simulated by GCM climate scenarios.

Köppens climate classification is too rough to examine differences between different data sources. Of

course, GHCN observations, CRU TS2.1 and VASCLIMO show considerable differences especially in semi-arid regions. Nevertheless, due to the sparse observation data it can not be determined which of the data sets is more reliable.

Regions of similar rainfall characteristics

The comparison between CRU TS2.1, VASCLIMO and GHCN data hints that there is good reason to use direct observations for defining characteristic regions with similar rainfall behaviour. In order to capture a complete rainy season in one SPI value, the GHCN data was accumulated for hydrological years, which cover the months Aug-Dec of the preceding year and Jan-Jul of the current year. The SPI values can be collected over different time periods in order to examine time-scale dependent behaviour, but in the north-western Maghreb, a rain season consists usually of maximum 10-14 single rainfall events, thus, series of monthly values, for example, quite often contain zero precipitation and reduce the quality of the SPI algorithm. Additionally, dry conditions in north-western Africa are in general only seen as dangerous, when they persist over two or more years. For these practical considerations, we focus only on annual sums of hydrological years.

A PCA has been applied to the SPI values. Figures 4 and 5 show the results. After Preisendorfers Rule N (Preisendorfer, 1988) only the first three principal patterns (PP) can be distinguished from random noise (Fig. 5). These PPs represent the Atlantic (ATL, PP01), the semi-arid/desert region south of the Atlas Mountains (SOA, PP02) and the Mediterranean (MED, PP03).

For the following steps, rainfall indices were constructed for these three regions for all data sets. For that purpose, rainfall was accumulated in the region and then SPI values were calculated. The first observations in GHCN data started – in the MED region – in 1841, but are neither reliable nor complete. It turned out that, in principle, GHCN data before 1931 are critical for further analyses. Despite this fact, we have chosen the period 1901-2007 of the GHCN data in order to compare the SPI series to CRU TS2.1. Results of the SPI calculation are presented in Fig. 6 (GHCN), Fig. 7 (CRU TS2.1) and Fig. 8 (REMO). An outstanding feature of the SPI series is the decrease of the index in the MED region since the mid-1970s. This has already been stated in Knippertz et al. (2003) and seems not to be induced by inhomogeneous or corrupt data, since it is also visible from independent climate station data, which contributed also to CRU TS2.1 (Fig.7). In general, GHCN and CRU TS2.1 are in good agreement.

In Fig. 8, SPI values from REMO climate scenario data are shown. In order to increase the reliability of the statistical procedure, all data were collected into one 422-years data set. Here, year 1-41 belong to the first 1961-2000 experiment, year 42-88 to the second, year 83-123 to the third, year 124-173 to the first 2001-2050 A1B-experiment and so on. This is also necessary because SPI values can not be compared when calculated from different time periods, since changes in the median of the distribution of rainfall values would be omitted. Fig. 8 shows an overview over the time series. The partly different behaviour of the scenario experiments can be clearly seen. A1B-1 and A1B-2 seem to show a strong

rainfall decrease; and the B1 scenarios are in general wetter but still have a drying trend. This is in good agreement of what one would expect from the results of the climate classification.

4. Results: Occurrences of wet and dry periods

The SPI series of GHCN stations, of CRU TS2.1 and of REMO are analyzed with respect to return values in the ATL, MED and SOA regions. First, the technique is elucidated using the GHCN data as an example, then only the results of the application on the other data are shown.

A fit to the data by a theoretical function is of interest, if the length of a data series is not sufficient to describe higher return times or values. In our case, the data permit the direct estimation of return times using empirical cumulative distributions (ECD and kernel estimated cumulative distribution, KCD) at a maximum of about 100 years, which allows for a comparative evaluation of the GPD based return time estimates.

The length of the SPI series determines the limits of maximum and minimum extremes. If we assume that the SPI follows perfectly a Gaussian normal distribution, the maximum absolute value of the SPI of a series of length 100 would be about 2.3, series with 1000 members would allow an extreme value of 3. In practice, the SPI distribution is a random sample and never perfect, thus, slightly larger values may occur or the limits may even not be reached. Nevertheless, SPI values of longer time series, which exceed the limits of a shorter series, should occur with higher return periods as can be derived from the shorter series.

The method we use for extreme value analysis is the so-called peak-over-threshold (POT) method. Any data from the tail of a distribution above a certain threshold are treated as a sample of Pareto-distributed data. Only for the purpose of uniform depiction, we changed the sign of dry SPI from negative to positive in the diagrams. GPD fits and estimates of return times and values are very sensitive to the threshold chosen. Sometimes, even subjective criteria like the by-eye-fit are used. One of the most preferred methods is the analysis of the mean excess function (also known as mean residual life, MRL, function), which is given in eq. (A.17) and is plotted in our results in order to estimate the quality of the threshold choice. The threshold was chosen by minimizing the mean integrated standard error (MISE. eq. A.18) of the quantile-quantile-plot. Figure 9 shows the GPD fit and the estimation of return times for the GHCN data. It contains three types of plots: the MRL and MISE functions in order to elucidate the choice of the threshold value. In the second column, the EDF, ECD, and the related kernel estimation distributions are plotted together with scaled GPD-fits of the tails. The right two columns show return value plots for extreme SPI values. In addition to the calculation of return values from a GPD fit, the more conventional method of inverting the Gaussian kernel estimation is undertaken. The results show clearly, that the GPD-based estimates of the return times contain large uncertainty even in the range where still data values are present (between 20 and 80 years) in the sample data. This is due to the fact that the estimated error of GPD parameters in eq. (A.15) is increasing with smaller numbers of available data. Possibly, longer time series would

improve the GPD estimate. The return values obtained from ECD and KCD coincide surprisingly well. A simple extrapolation of the KCD return values seems to be more reliable than the GPD-based estimation. On the other hand, we see that the SPI values of the GHCN data is not perfectly Gaussian distributed; mainly due to the shortness of the series accompanied by a large interannual variability. The large error of the GPD fit advises against overestimating the statistical quality of the data used. By comparison, the extreme value analysis shows that dry excesses with a SPI level of 1.3 (ATL) to 1.7 (SOA) occur every 10 years. SPI values of 2.5 occur in observations every 100 years, because this is the maximum value in original data due to the limited number of observations. In dry cases, the optimum choice of the threshold of the GPD corresponds to a return value of about 20 years, only in the wet case and for MED and SOA it is below 10 years. This indicates that wet period recurrences have a larger uncertainty in these two regions. The 95% uncertainty range at the 100 years return value of the SPI is between 1.7-3 (SOA dry) and 1.5-4 (ATL dry, ATL wet and MED wet).

The same procedure has been applied to CRU TS2.1 and to RCM data. The RCM data were analyzed in subsets for three periods: 1962-2050, 1962-2000, and 2031-2050. Remember that we have always used the hydrological year, i.e. the month Aug-Dec of the preceding year and Jan-Jul of the present year. The results are presented in Fig. 10. Three outstanding features result from this graph: (1) The return values of the SPI from the whole RCM time series are very similar to GHCN return values. This is a consequence of the normalization; the model SPI data may represent another absolute rainfall value. Thus, the model bias is hidden. (2) For the 1961-2000 data, the REMO model dry bias results not in an enhancement of dry periods or in a weakening of wet periods; in fact dry SPI values have smaller return times than observational SPI values. This is not surprising, because the SPI mean shifts with the dry bias towards smaller rainfall rates. (3) For wet SPI values, observation data and model scenarios do not show large deviations for both present day and climate scenarios.

Although the model bias is hidden due to the SPI calculation, one has to keep in mind that SPI values of the RCM may represent totally different absolute rainfall amounts. In principle, rainfall sums are a nonlinear function of the SPI values and can be calculated. But the variability of both SPI and absolute rainfall inside the regions is very large, thus, we forego presenting such values because they are difficult to interpret.

The future assessment of return values presented in the right two panels of Fig. 10 reveals a pronounced enhancement of the frequency of dry periods, whereas the occurrence of wet periods is in general unchanged. When we look at absolute values, the differences of return times are quite large. In example, the recurrence time for a dry SPI value of 2.0 in the ATL region is from RCM runs for present day condition 100 years (GPD estimation) or and 110 years from kernel estimation. In the climate scenario for 2031-2050, the same SPI value has a recurrence time of 15 years in both GPD and kernel estimation. The other two regions show the same magnitude in differences of present day and future return times of the dry SPI values. Thus, the climate change represented by the RCM scenarios has to be called dramatic, at least with respect to interannual rainfall variability. Once more, this shows

clearly that the climate change due to GHG forcing results not solely in a reduction of rainfall and in near surface warming, but also in a modification of rainfall variability, which results most likely from changes in occurrences of weather regimes. However, from this merely statistical analysis we cannot delve into deeper detail here.

Conclusions

The actual climate in the north-western Maghreb, mainly in Morocco, has been examined with respect to dry and wet periods in the 20th century. The data used were GHCN rainfall observations and CRU TS2.1 gridded rainfall. The future climate conditions, also focussing on the occurrence of dry and wet conditions, have been assessed using regional climate model data obtained by SRES A1B and B1 climate scenarios and present day model runs with REMO. It has been found by Köppen climate classification that the tendency towards dryer and warmer climates, which has been observed in the 20th century, is continuing and amplified in the climate scenarios. The climate classification also revealed a remarkable model bias of REMO towards dryer conditions.

For assessing wet and dry conditions in somewhat heterogeneous regions, areas with similar rainfall characteristics have been defined using a PCA. Three regions emerged from first three eigenvectors (principal patterns) of the PCA: The Atlantic (ATL), the Mediterranean (MED) and the semi-arid and arid region south of the Atlas Mountains (SOA). The remaining principal patterns do not emerge from random noise.

In order to compare results from our different sources, a normalization of rainfall data using the standardized precipitation index (SPI) has been undertaken. The occurrences of wet and dry periods have been examined using extreme value analysis using a fit of the general Pareto distribution to the SPI values above a certain threshold. The GPD fit was compared to simple approaches like direct inversion of empirical distributions and distribution obtained from Gaussian kernel estimation. The study revealed that CRU TS2.1 and GHCN data were – as expected – in good agreement. Return times of the SPI obtained from the complete data of the REMO RCM scenarios are similar to the values of observed data, which is a consequence of the normalization. Present day RCM data showed reasonably larger recurrence times of dry SPI values than future scenarios and GHCN observations. The future scenario data for 2031-2050 clearly showed more frequent occurrences of dry periods in all regions and nearly unchanged wet period occurrences in the ATL and SOA regions. In the MED region, the wet period frequencies seem reduced in RCM scenarios. The comparison of GPD analysis with kernel estimation showed the strong uncertainty of GPD approaches. Even for “known” conditions, where the kernel estimation is relatively reliable, the error of GPD fits is very large. On the other hand, this might suggest that any climatic rainfall data has strong random noise and that even kernel estimates are not as statistically reliable as they may seem. Nevertheless, the good agreement of return values obtained by the EDF and the kernel estimated distribution, which is regardless to the large standard error between them, supports the clear statement that the kernel estimated return values are at least in

the range covered by the EDF more reliable than a GPD fit. One reason for the poor quality of GPD fits is that the SPI data may not be perfectly Gaussian distributed, although they underwent a rough process of normalization. For example, higher frequencies of a low number of characteristic weather regimes may result in a multimodal distribution.

Nevertheless, estimated return values of RCM and observational data are in good agreement. This fact justifies the statement that the GHG forcing of climate change will result in a strengthening of the present stress conditions due to water shortcomings, both from the extrapolation of observed trends and from RCM data.

The results of our study have to be slightly qualified. Since no other set of RCM scenarios covering Northern Africa with such a high resolution exists, the issue of future climate research on regional climate variability is to corroborate or refute the results of this RCM approach using other models. In addition, the coincidence of weather regimes and dry/wet conditions, which has been documented in Knippertz et al. (2003) has to be extended to RCM data. Separating SPI series according to different weather regimes into different, perfectly unimodal distributions might enhance the reliability of the GPD-based extreme value analysis.

Appendix

For the present study, some standard data analysis techniques were applied. Although most of these techniques are commonly used and have been described several times in the literature, details of the application differ very often. Therefore, in some studies it may be difficult to replicate the findings. In order to facilitate the recalculation, the statistical techniques used are briefly explained.

A. Distribution Functions

Three methods for describing randomly distributed data suggest themselves. The first is simply to calculate a histogram by collecting data in bins and subsequent normalization. In this article, we refer to the resulting distributions from this technique as empirical probability distribution (EPD) or empirical cumulative distribution (ECD). An EPD can be quite irregular and multimodal due to random characteristics. If we have a rough idea about the theoretical probability distribution function (PDF) of the basic population, we can try appropriate kernel density estimation. In the histogram, every data point increases the value of a corresponding bin by 1. Kernel density estimation adds for one data point an arbitrary shaped function to the distribution. The result is a smoother distribution than the EPD. In this article, Gaussian kernel density is estimated for the SPI by using a bell-shaped weight function. The distributions found by kernel density estimation are referred to as kernel estimated probability distribution (KPD) and kernel estimated cumulative distribution (KCD). In order find the best balance between smoothed and noisy distribution, optimal weight function widths are usually gained by minimizing the mean integrated squared error between KPD and EPD. But for our presentations the kernel density estimates were intentionally a little bit “oversmoothed”, because the

inverse KCD was used to calculate return values.

The third method to define a PDF from random data is to fit the distribution to a known theoretical distribution. This always involves approximation and special methods like the maximum likelihood estimation (MLE) or probability weighted moments like the L-moments (see Appendix D).

B. The principal Component Analysis (PCA)

Principal component analysis has been widely adapted in climate research. The intention is to define coherent patterns of variability of a data set in either time or space. The PCA defines a set of – in a statistical sense – independent (orthogonal) patterns of variability. The technique of PCA has been introduced by Pearson (1901). Hotelling (1933) improved the PCA, since about 30 years it has frequently been used in climate research. Preisendorfer (1988) gives a detailed overview over PCA techniques. The PCA in this study was implemented using a freely available software package from Murtagh (2007).

The central issue of the PCA is the diagonalization of a symmetric covariance or correlation matrix. For that purpose, data are stored in a matrix D with the elements $\{d_{ij}, i \in (1,\ldots,N), j \in (1,\ldots,M)\}$ with time-series of N points in time, stored in columns, at M locations in space. In the following, upper case letters describe 2-dimensional tensors, the superscript T behind the matrix denotes the transformation (changing rows and columns) of a matrix. The covariance matrix of the time series is now

$$C_t = D^T D \qquad \textbf{(A.1)}$$

and the covariance matrix in space is

$$C_s = DD^T \qquad \textbf{(A.2)}$$

C_t and C_s are symmetric matrices of dimension M and N, respectively. Note that if D is built from standardized anomalies, D^TD and DD^T contain correlations. The next step is the solution of the eigenvalue-problem

$$D^T DB = B\Lambda \quad or \quad C_t B = B\Lambda \qquad \textbf{(A.3)}$$

or, by solving the adjoint problem

$$DD^T A = A\Lambda \quad or \quad C_s A = A\Lambda \qquad \textbf{(A.4)}$$

Here, Λ is the diagonal matrix which contains in the i-th diagonal element the eigenvalue $\{\lambda_i, i \in (1,\ldots,\min(N,M)\}$. The columns of A and B contain a set of orthogonal eigenvectors in space and a set of eigenvectors in time, respectively. λ_i is attached to the i-th eigenvector e. g. $\{b_{ki}, k \in (1,\ldots,\min(N,M)\}$ of B. Interestingly, Eq. (A.4) can be derived by multiplying D from the left to both sides of Eq. (A.3), thus, the eigenvalues of Λ in (A.3) and (A.4) are identical. The solution of a properly posed eigenvalue problem, i. e. $\det(D^TD) > 0$, is unique except to a scalar factor for each eigenvector. Usually, one of the eigenvector-matrices is normalized, so that the length of the vectors in columns is 1. In case B is normalized, we have $B^TB = I_M$ (unity matrix) and $AA^T = \Lambda$. In this case, the relation between time- and space-eigenvectors is

$$A = \Lambda DB \quad or \quad D^T A \Lambda^{-1} = B \qquad \textbf{(A.5)}$$

The eigenvalues in Λ are ordered by value. The relative portion ($\lambda_i / \sum\lambda_i$) represents the explained variance of the i-th eigenvector. An advantage of the freedom of choice between the eigenvalue systems (A.3) and (A.4) is that one can take the form of the problem with smaller dimensions, since the rank of D^TD and DD^T is at maximum min(N,M). If the data is highly correlated – what is desirable in order to detect patterns of variability – the rank can even be smaller, which makes the system possibly not uniquely solvable. Fortunately, this in practice is no problem for the most solvers; eigenvalues connected to dimensions which are not contained in the image of D^TD or DD^T contain just numerical noise. This can be detected easily because they are very often negative, what should not happen because covariance/correlation matrices are symmetric and, thus, have only positive eigenvalues. Usually, only a part of the eigenvectors represents significant correlation patterns. A general and objective identification of significant patterns is not as easy, thus, for this purpose Monte-Carlo-Experiments are used. In this study, 1000 experiments with uncorrelated, gamma-distributed data series computed with the same parameters of the Gamma distribution as the rainfall observations were conducted. Eigenvalues were calculated using the same PCA technique as for observational data. We know that the resulting eigenvalues represent random noise. Preisendorfer (1988) has formulated the so-called Rule N, which says that only these eigenvectors represent significant patterns whose eigenvalues emerge clearly from random eigenvalues. In our application, Fig. 5 shows that only three eigenvectors seem to emerge from random noise.

C. The Standardized Precipitation Index (SPI)

Rainfall is very heterogeneous in time and space. Therefore, e. g. temporal variations of rainfall series at different locations are not directly comparable. One method to overcome this problem is to normalize the data. Since rainfall distributions are in general skewed, normalization with mean, variance or standard deviations is often insufficient. Some different indices have been found to be acceptable in the science community. The WMO (1983) recommends using the Quintile index (QI) defined as Knippertz et al. (2003) did, but the QI is a discrete index value and its variability depends, when spatial averages are calculated, too much on the number of available stations. One of the more prominent indices is the Palmer drought severity index (Palmer, 1965). The only drawback of the Palmer index is that it needs additional information like evaporation and temperature, which is not always achievable. For that reason, we decided to use the SPI, which was first introduced by McKee et al. (1993) and is used widely for drought detection. The SPI is calculated solely from rainfall values.

A motivation for defining the SPI was that especially dry periods are hard to detect from direct rainfall observations. Rainfall PDFs are usually skewed with a shorter tail at smaller values. Additionally, the lower values are bound by zero precipitation. Therefore, the gamma distribution is often used to describe time series of cumulative rainfall on scales of weeks to years. The basic idea of the SPI is to define an index which follows a Gaussian normal distribution. Such index fulfils two requirements: It

enables an easier analysis of the dry part of rainfall distributions, and it allows comparing rainfall characteristics at different locations which is often problematic due to the heterogeneity of rainfall observations.

The procedure to compute SPI from rainfall series is straight forward. First, parameters of a theoretical probability distribution function (PDF) – in our case the Gamma distribution – are fitted to the empirical distribution. Second, the rainfall observations are mapped to values of the estimated cumulative distribution function (CDF) of the Gamma distribution. Third, an equal probability transformation to the CDF of the Gaussian normal distribution is applied.

Let X = {x_j, j=1…N} be a realization of a Gamma-distributed random quantity. The theoretical Gamma PDF is described by two parameters *a* (shape parameter) and *b* (scale parameter):

$$g(x,a,b) = \frac{x^{a-1}b^{a}}{\Gamma(a)}\exp(-bx) \qquad \textbf{(A.6)}$$

$\Gamma(a)$ is the Gamma-Function. The parameters can be estimated from MLE in an approximation after Choi and Wette (1969):

$$\hat{a} = 3 - v + \frac{\sqrt{(v-3)^2 + 24v}}{12v} \quad with \quad v = \ln\left(\frac{1}{N}\sum_{j=1}^{N} x_j\right) - \frac{1}{N}\sum_{j=1}^{N} x_j$$
$$\hat{b} = \frac{1}{\hat{a}}\frac{1}{N}\sum_{j=1}^{N} x_j \qquad \textbf{(A.7)}$$

The hats denote that the values are estimated from one realization. Defining $t=x/b$, the CDF of the Gamma distribution is the incomplete gamma function:

$$G(x,a,b) = \int_0^x g(x,a,b)\,dx = \frac{1}{\Gamma(a)}\int_0^x t^{a-1}e^{-t}dt \qquad \textbf{(A.8)}$$

G is easily calculated via numerical integration. It has turned out that for our intention no further approximations were necessary. By means of $G(x_j)$, the SPI at point x_j is calculated by:

$$SPI(x_j) = Errf^{-1}(G(x_j)) \qquad \textbf{(A.9)}$$

$Errf^{-1}$ is the inverse of the CDF of the Gaussian normal distribution, which can be taken either from tables or from approximation formula. It should be mentioned that applying an additional spatial average on the SPI demands a new normalization. Thus, the SPI values were calculated from spatially accumulated rainfall in our regions of interest.

D. Extreme Value Analysis using the Generalized Pareto Distribution (GPD)

The extreme value analysis is done using the so-called partial duration or peak-over-threshold (POT) series. This technique is widely accepted (see e. g. Paeth and Hense, 2005, or Bordi et al., 2006) and uses the partial set of data of a series, which exceeds a certain limit. For any random sample X = {x_j, j=1,…,N}, it has been shown that for a properly behaving (i. e. invertible and continuous) EPD, tails above a sufficiently large threshold can be represented by a GPD (Balkema and de Haan, 1974). The

GPD is a three-parameter distribution with probability density

$$f(x,a,b,c)=\begin{cases}\frac{1}{b}\left(1+a\frac{x-c}{b}\right)^{-\frac{1+a}{a}} & for\ a\neq 0\\ \frac{1}{b}e^{-\frac{x-c}{b}} & for\ a=0\end{cases} \qquad \textbf{(A.10)}$$

and the cumulative distribution function

$$F(x,a,b)=\begin{cases}1-\left(1+a\frac{(x-c)}{b}\right)^{-\frac{1}{a}} & for \quad a\neq 0\\ 1-e^{-\frac{x-c}{b}} & for \quad a=0\end{cases} \qquad \textbf{(A.11)}$$

The GPD is described by the location parameter *c*, the scale parameter *b* and the shape parameter a. It is defined for any value $x > c$ for $a > 0$ and $c \le x \le c - b/a$. *F(x,a,b,c)* is the probability that a value in the tail of an EPD is larger than *c* and smaller than or equal to *x*. The GPD is an exponential distribution for $a = 0$, a type II Pareto distribution for $a < 0$ and an ordinary Pareto distribution for $a > 0$. The estimation of parameters of the GPD is not analytically possible; a brief overview of methods is given in Singh and Guo (1995). In this study, the method of L-moments (Hosking and Wallis, 1987) has been used. For that purpose, probability weighted moments β_m, m=0,..,2 were calculated:

$$\beta_0=\frac{1}{N}\sum_{j=1}^{N}x_j$$
$$\beta_m=\frac{1}{N}\sum_{j=m+1}^{N}\frac{(j-1)(j-2)...(j-r)}{(N-1)(N-2)...(N-r)}x_j \qquad \textbf{(A.12)}$$

From these moments, the L-moments have been computed:

$$\lambda_1=\beta_0$$
$$\lambda_2=2\beta_1-\beta_0 \qquad \textbf{(A.13)}$$
$$\lambda_3=6\beta_2-6\beta_1+\beta_0$$

The parameters of the GPD were estimated by:

$$a=\frac{\lambda_2-3\lambda_3}{\lambda_2+\lambda_3}$$
$$b=\lambda_2(1+a)(2+a) \qquad \textbf{(A.14)}$$
$$c=\lambda_1-\frac{b}{1+a}$$

The location parameter c is usually, except from numerical fluctuations, identical with the lowest value of $\{X|x_j > c\}$. Hosking and Wallis (1987) proved that for a large number of samples maximum likelihood estimates of *a* and *b* are normally distributed. The estimation error *a* and *b* is expressed in the approximated covariance matrix of *a* and *b*:

$$\begin{pmatrix} \overline{a'^2} & \overline{a'b'} \\ \overline{a'b'} & \overline{b'^2} \end{pmatrix} = \frac{1}{N}\begin{pmatrix} (1+a)^2 & b(1+a) \\ b(1+a) & 2b^2(1+a) \end{pmatrix} = \begin{pmatrix} \sigma_a^2 & \sigma_{ab}^2 \\ \sigma_{ab}^2 & \sigma_b^2 \end{pmatrix} \quad \textbf{(A.15)}$$

Here, the overbar denotes an average over the sample of (*a*,*b*). This error estimate may be a little bit smaller for L-moments, but has been used to ensure that we are on the safe side. The error of the GPD can now easily be derived from multivariate error propagation of the GPD *f*:

$$\sigma_f^2 = \left(\frac{\partial f}{\partial a}\right)^2 \sigma_a^2 + \left(\frac{\partial f}{\partial b}\right)^2 \sigma_b^2 + 2\left(\frac{\partial f}{\partial a}\frac{\partial f}{\partial b}\right)\sigma_{ab}^2 \quad \textbf{(A.16)}$$

The estimation of the optimum threshold for the GPD fit is very important for reliable results. It has been shown that the mean residual life function (MRL, also known as mean excess function) has a linear shape for sufficiently high thresholds. The MRL function is defined as:

$$MRL(\theta) = \frac{1}{N_{ex}(\theta)} \sum_{i=1}^{N_{ex}(\theta)} (x_i - \theta) \quad \textbf{(A.17)}$$

θ is the threshold, $N_{ex}(\theta)$ is the number of values exceeding θ. Because the fit is – in a statistically sense – better when using more data, the threshold should be chosen to be in the linear range of the MRL function, but as near to the centre of the distribution as possible. This is a somehow arbitrary criterion, thus, the MRL was used in this study merely to control the estimation of the optimum threshold.

Another method to estimate the threshold is based on the so-called quantile-quantile plot (QQ-plot). In a QQ-plot, empirical cumulative probabilities are plotted against the GPD fit based on this threshold. Supposed we have sufficiently GPD distributed sample data, the perfect fit would result in a straight line of identity. A quality measure for the GPD fit is the mean integrated standard error (MISE):

$$MISE(\theta) = \sum_{i=1}^{N_{ex}(\theta)} (F(x_i, a, b) - ECD(x_i))^2 \quad \textbf{(A.18)}$$

Here, ECD is the empirical cumulative distribution function. The MISE is – except to a constant factor – a measure for the distance of the points from the line marking the identity. In our estimation of θ, the threshold according to the minimum value of MISE for moving θ has been chosen.

The return levels are calculated from the inverse of the cumulative GPD Function. The probability, that a random value x_j taken from our sample in size N exceeds the threshold *c* is

$$p_c = P(x_j > c) = \frac{N_{ex}}{N} \quad \textbf{(A.19)}$$

The probability, that values in a GPD fit exceed an arbitrary value s >= *x* is

$$P(x_j > s \mid x_j > c) = \left(1 + a\frac{x-c}{b}\right)^{-\frac{1}{a}} \quad \textbf{(A.20)}$$

This can be converted to

$$P(x_j > s) = p_c\left(1 + a\frac{x-c}{b}\right)^{-\frac{1}{a}} \quad \textbf{(A.21)}$$

The level x_t that in average is exceeded once in a time interval of t is the inversion of eq. (A.21):

$$x_t = c + \frac{b}{a}\left\{(tp_c)^a - 1\right\} \quad \textbf{(A.22)}$$

Again, the standard error of x_t obtained from error propagation in eq. (A.16).

$$\sigma_{x_t}^2 = \left(\frac{\partial x_t}{\partial a}\right)^2 \sigma_a^2 + \left(\frac{\partial x_t}{\partial b}\right)^2 \sigma_b^2 + 2\left(\frac{\partial x_t}{\partial a}\frac{\partial x_t}{\partial b}\right)\sigma_{ab}^2 \quad \textbf{(A.23)}$$

with

$$\frac{\partial x_t}{\partial a} = \frac{b}{a}\left\{\frac{1}{a} + \left(\log(tp_c) - \frac{1}{a}\right)(tp_c)^a\right\}$$
$$\frac{\partial x_t}{\partial a} = \frac{1}{a}\left((tp_c)^a - 1\right) \quad \textbf{(A.24)}$$

The programs used in the present study to calculate the GPD fit are freely available under https://wiki.uni-koeln.de/kerschgens/index.php/Kai_Born.

E. List of Abbreviations and Acronyms

The list is in alphabetical order.

ATL	Atlantic coast region
CDF	Cumulative distribution function
CRU	Climate research unit of the university of East Anglia
CRU TS2.1	An observational climate data set provided by the CRU
ECD	Empirical cumulative distribution
ECHAM	European Center for Medium Ragne Weather forecast model – Hamburg version
ENSO	El Niño-Southern Oscillation
EPD	Empirical distribution function
FAO	Food and Agriculture Organization of the United Nations
GCM	General circulation model
GHCN	Global historical climatology network, produced jointly by the National Climatic Data Center and Carbon Dioxide Information Analysis Center at Oak Ridge National Laboratory
GHG	Greenhouse gas
GPD	Generalized distribution function
IMPETUS	***I**ntegratives **M**anagement-**P**rojekt für einen **e**ffizienten und **t**ragfähigen **U**mgang mit **S**üßwasser in Westafrika* An Integrated Approach to the Efficient Management of Scarce Water Resources in West Africa
IPCC	Intergovernmental Panel on Climate Change
KCD	Kernel estimated cumulative probability distribution
KPD	Kernel estimated probability distribution
LCC	Land cover changes
MED	Mediterranean cost region
MISE	Mean integrated standard error
MLE	Maximum likelihood estimation
MPIfM	Max Planck Institute for Meteorology, Hamburg
MRL	Mean residual life function
NAO	North Atlantic Oscillation
NCAR	National Center for Atmospheric Research, Boulder, Colorado, USA
NCEP	National Centers for Environmental Predictions, Camp Springs, Maryland ,USA

OAGCM	Ocean-Atmosphere general circulation model
PCA	Principal component analysis
PDF	Probability distribution function
POT	Peak-over-threshold method: only values exceeding a fixed threshold are taken into consideration
PP	Principal pattern
QI	Quintile index
QQ-plot	Quantile-quantile plot
RCM	Regional climate model
REMO	Regional Model: A meso-sale amospheric model for regional climate modelling applications
SOA	South of the Atlas region
SPI	Standardized precipitation index
SRES	Special Report on Emissions Scenarios of the IPCC
SST	Sea Surface Temperature
SYNOP	Synoptic weather observations
VASCLIMO	Variability Analysis of Surface Climate Observations: A joint project between the German Weather Service DWD and the Institute for Meteorology and Geophyiscs, Johann Wolgang Goethe University Frankfurt

Acknowledgements

This work was part of the IMPETUS West-Africa project and was supported by the Federal German Ministry of Education and Research (BMBF) under grant No. 01 LW 06001A in the GLOWA programme and by the Ministry of Innovation, Science, Research and Technology (MIWFT) of the federal state of Northrhine-Westfalia under grant No. 313-21200200.

The observational data were collected and maintained under the participation of Tim Brücher and Kristina Piecha from the Institute for Geophysics and Meteorology of the University Cologne. The SPI analysis has been supported by the work of Rabea Haas, University of Cologne. Robin Girmes and Kai-Oliver Heuer, who were involved in the IMPETUS project, have supplied model data management. Daniela Jacob and Ralf Podzun, Max-Panck-Institute for Meteorology in Hamburg, have realized the RCM model runs at the *Deutsches Klimarechenzentrum*. We are grateful to two anonymous reviewers for their rewarding comments.

References

Beck, C., J. Grieser, B. Rudolf, 2005: A New Monthly Precipitation Climatology for the Global Land Areas for the Period 1951 to 2000. Published in *Climate Status Report* 2004, pp. 181 - 190, German Weather Service, Offenbach, Germany.

Balkema, A. A., L. de Haan, 1974: Residual life time at great age. -- *Annals of Probability* ***2***, 792-804.

Bordi, I., A. Sutera, 2001: Fifty years of precipitation: Some spatially remote teleconnections. -- *Water Res. Management*, **15**, 247-280.

Bordi, I., K. Fraedrich, M. Petitta, A. Sutera, 2006: Extreme value analysis of wet and dry periods in Sicily. -- *Theor. Appl. Climatol.* (2006), DOI 10.1007/s00704-005-0195-3.

Choi, S. C., R. Wette, 1969: Maximum Likelihood Estimation of the Parameters of the Gamma Distribution and Their Bias. -- *Technometrics*, **11**(4), 683-690-

El Hamly, M., Sebbari, R., Lamb, P. J., Ward, M. N., D. H. Portis, 1998: Towards the seasonal prediction of Moroccan precipitation and its implication for water resources management. -- Water Resources Variabilty in Africa during the XXth century, Proceedings of the Abidjan 1998 Conference, Abidjan, Côte d'Ivoire, 1998. IAHS Publ. No. 252, 79-87.

Emberger, L., 1930 : La végétation de la région méditerranéenne; essai de classification des groupements végétaux. 1930. -- *Rev. Gen. de Bot.*, **42**, 641-662.

Emberger, L., 1955 : Une classification biogéographique des climats. -- *Recueil Trav. Lab. Bot. Géol. Zool. Fac. Sci. Univ. Montpellier*, Serie Bontanique, **7**, 3-43.

Finckh, M., A. Augustin, N. Jürgens, 2007: Monitoring biodiversity on the Saharan slopes of the High Atlas, Morocco. -- *Mountain Forum Bulletin* **2007 (1)**, 3-4.

Fraedrich, K., F.-W. Gerstengarbe, P. C. Werner, 2001: Climate shift during the last century. --*Climatic Change*, **50**, 405-417.

Griffiths, F., 1972: The Mediterranean Zone. -- Chapter 2 in *World Survey of Climatology Vol* ***10:*** *Climates of Africa.* Ed. H. E. Landberg. Elsevier Publishing Company Amsterdam – London – New York, 37-74.

Griffiths, F., K. H. Soliman, 1972: The Northern Desert (Sahara). -- Chapter 3 in *World Survey of Climatology, Vol* ***10:*** *Climates of Africa*. Ed. H. E. Landberg. Elsevier Publishing Company Amsterdam – London – New York, 75-132.

Guetter, P. J., Kutzbach, J. E., 1990: A modified Koeppen classification applied to model simulations of glacial and interglacial climates. -- *Clim. Change*, **16**, 193-215.

Guttmann, N. B., 1999: Accepting the standardized precipitation index: a calculation algorithm. -- *J. Amer. Water Resources Assn.*, **35**, 311-322.

Hosking, J., J. Wallis, 1987: Parameter and quantile estimation for the generalized Pareto distribution. -- *Technometrics*, **29**, 339-349.

Hotelling, H., 1933: Analysis of a complex of statistical variables into principal components. -- *J. Educ. Psychol.*, **24**, 417-441.

IPCC, 2007: IPCC Fourth Assessment Report (AR4) Working Group I Report "The Physical Science Basis", available online http://ipcc-wg1.ucar.edu/wg1/wg1-report.html (Sep 16, 2007).

Jacob, D., Van den Hurk, B.J.J.M., Andrae, U., Elgered, G., Fortelius, C., Graham, L.P., Jackson, S.D., Karstens, U., Koepken, C., Lindau, R., Podzun, R., Rockel, B., Rubel, F., Sass, B.H., Smith, R., Yang, X., 2001, A comprehensive model intercomparison study investigating the water budget during the PIDCAP period. -- *Meteorol. Atmos. Phys.* **77**, 19-44.

Jung, T., L. Ferranti, A. M. Tompkins, 2006: Response of the Summer of 2003 Mediterranean SST Anomalies over Europe and Africa. -- *J. Climate* **19**, 5439-5454.

Knippertz, P.; Christoph, M.; Speth, P., 2003: Long-term precipitation variability in Morocco and the link to the large-scale circulation in recent and future climates. -- *Meteorology and Atmospheric Physics*, **83**, 67–88.

Knippertz, P., 2004: A simple identification scheme for upper-level troughs and its application to winter precipitation variability in Northwest Africa. -- *J. Climate*, **17**, pp. 1411-1418.

Köppen, W., 1936: Das geographische System der Klimate. -- In: Handbuch der Klimatologie, Vol. 1, Part C, Gebr. Bornträger Verlag Berlin, 388 pp. (in German)

Kottek, M., J. Grieser, C. Beck, B. Rudolf, F. Rubel, 2006: World map of the Köppen-Geiger climate classification updated. -- *Meteorol. Z.*, **15**, 259-263.

Lamb, P.J., R. A. Peppler, 1987: North Atlantic Oscillation: concept and application. -- *Bull. Amer. Met. Soc.* **68**, 1218–1225.

Lamb P.J, M. El Hamly, D. H. Portis DH, 1997: North-Atlantic Oscillation. -- *Géo Observateur* **7**, 103–113.

Li, S., W. A. Robinson, S. Peng, 2003: Influence of the North Atlantic SST tripole on northwest African rainfall. -- *J. Geophys. Res.* **108(D19)**, ACL 3, 1-20, doi: 10.1029/2002JD003130.

McKee, T. B., N. J. Doesken, J. Kleist, 1993: The relationship of drought frequency and duration to time scales. -- *Preprints, 8th Conference on Applied Climatology*, Jan. 17-22, Anaheim, CA, 179-184.

Mitchell, T. D., P. D. Jones, 2005: An improved method of constructing a database of monthly climate observations and associated high resolution grids. -- *Int. J. Climatol.* **25**, 693-712.

Murtagh, F., 2007: Multivariate Data Analysis Software and Resources. -- Available under http://astro.u-strasbg.fr/~fmurtagh/mda-sw/, 25.8.2007.

Nicholson, S. E., 2000: The nature of rainfall variability over Africa on time scales of decades to millennia. -- *Global and Planetary Change* **26**, 137-158.

Paeth, H., 2004: Key factors in African climate change evaluated by a regional climate model. -- *Erdkunde* **58**, 290-315.

Paeth, H., K. Born, R. Podzun, D. Jacob, 2005, Regional dynamic downscaling over West Africa: Model evaluation and comparison of wet and dry years. -- *Meteorol. Z.* **14**, 349-367.

Paeth, H., Hense, A., 2005: Mean versus extreme climate in the Mediterranean region and its sensitivity to future global warming conditions. -- *Meteorol. Z.* **14**, 329-347.

Paeth, H., K. Born, R. Girmes, R. Podzun, D. Jacob, 2008: Regional Climate change in tropical and northern Africa due to greenhouse forcing and land use changes. -- Accepted in *J. Climate*.

Palmer, W., 1965: Meteorological Drought. -- *Tech. Rep.* 45, U.S. Weather Bureau, Washington D.C., 58 pp.

Pearson, K., 1901: On lines and planes of closest fit to systems of points in space. -- *Philos. Magazine* **2**, 559-572.

Portis D. H., J. E. Walsh, M. El Hamly, P. J. Lamb, 2001: Seasonality of the North Atlantic Oscillation. -- *J. Climate* **14**, 2069–2078

Preisendorfer, R. W., 1988: Principal component analysis in meteorology and oceanography. -- In: C. D. Mobly (ed.), *Developments in Atmospheric Sciences*, **17**, 425 pp.

Roeckner, E. et al., 2003. The atmospheric general circulation model ECHAM 5. PART I: Model description.-- MPI-Report 349, 127pp (2003).

Singh, V, P., H. Guo, 1995: Parameter estimation for 3-parameter generalized pareto distribution by the principle of maximum entropy (POME). -- *Hydrological Sciences Journal* **40**, 165-181.

Vose R. S., R. L. Schmoyer, P. M. Steurer, T. C. Peterson, R. Heim, T. R. Karl, J. K. Eischeid, 1992: The Global Historical Climatology Network: Long-term monthly temperature, precipitation, sea level pressure, and station pressure data. -- NDP-041. Carbon Dioxide Information Analysis Center, Oak Ridge National Laboratory, Oak Ridge, Tennessee

Ward, M. N., P. J. Lamb, D. H. Portis, M. El Hamly, R. Sebbari, 1999: Climate variability in northern Africa: understanding droughts in the Sahel and the Maghreb. -- Chapter 6 in: *Beyond El Niño – decadal and interdecadal climate variability.* Ed.: A. Navarra. Springer Verlag, 119-140.

WMO, World Meteorological Organization, 1983: Guide to climatological practices. Secretariat of the World Meteorological Organization, Geneva, Switzerland. -- WMO No. 100, Second Edition 1983, 198 pp.

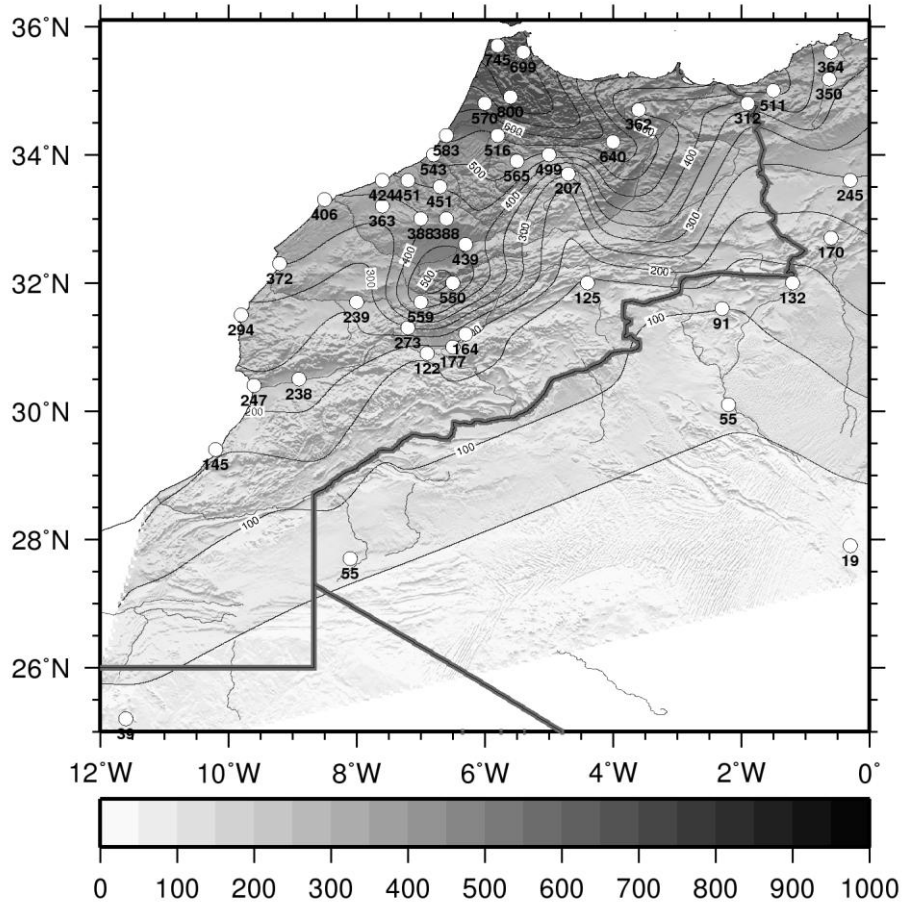

***Fig.1**: SYNOP Stations in the north-western Maghreb. Circles represent the locations of the stations, numbers the observed 1951-2000 mean annual rainfall sum in mm.*

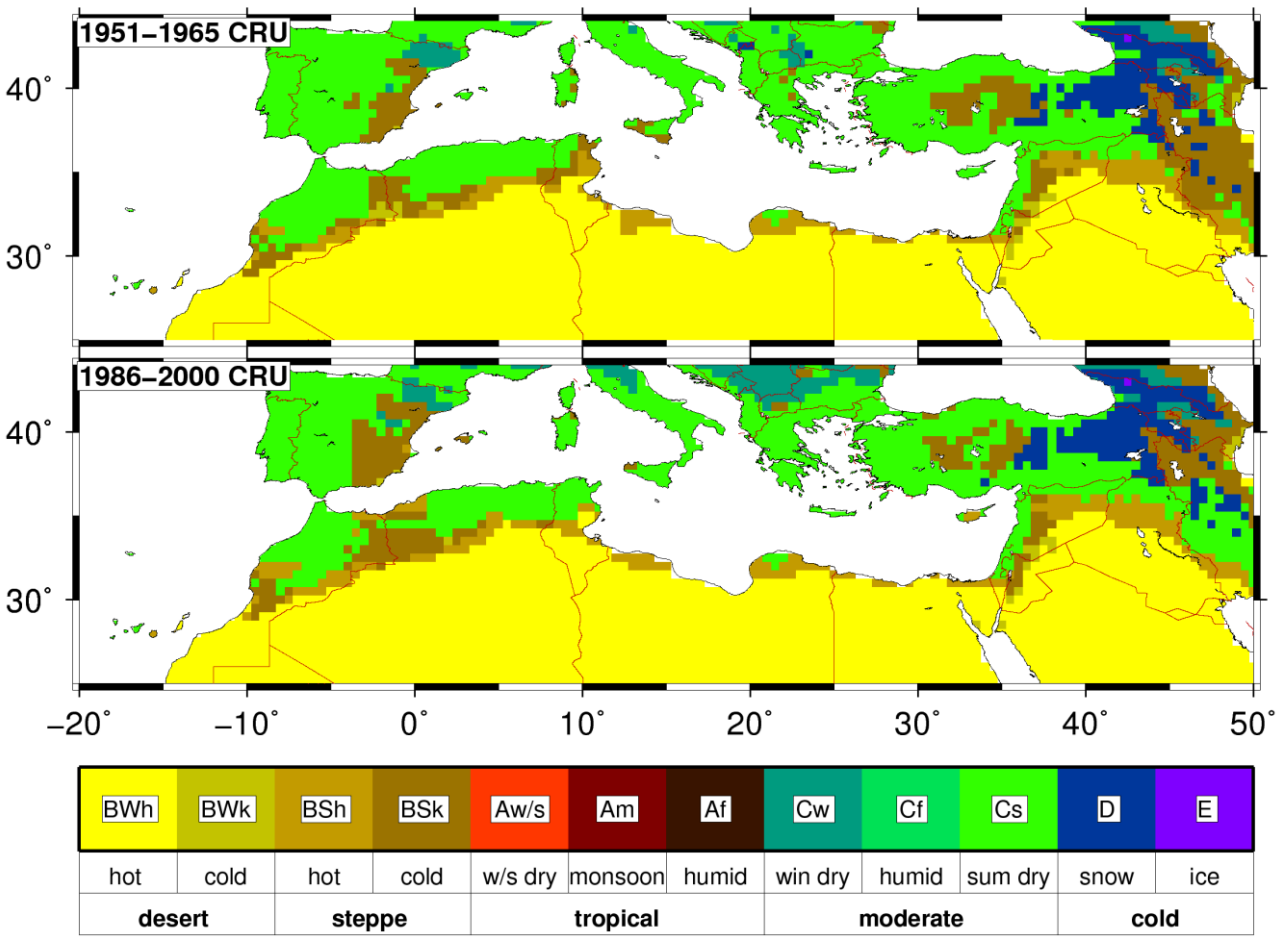

Fig. 2: *Climate classification after a reduced Köppen scheme applied to the CRU TS2.1 data. The maps compare the climate classes for 1951-1965 to 1986-2000 and reveal a trend towards dryer and warmer climates in the second half of the 20th century. Classification criteria are listed in Table 1.*

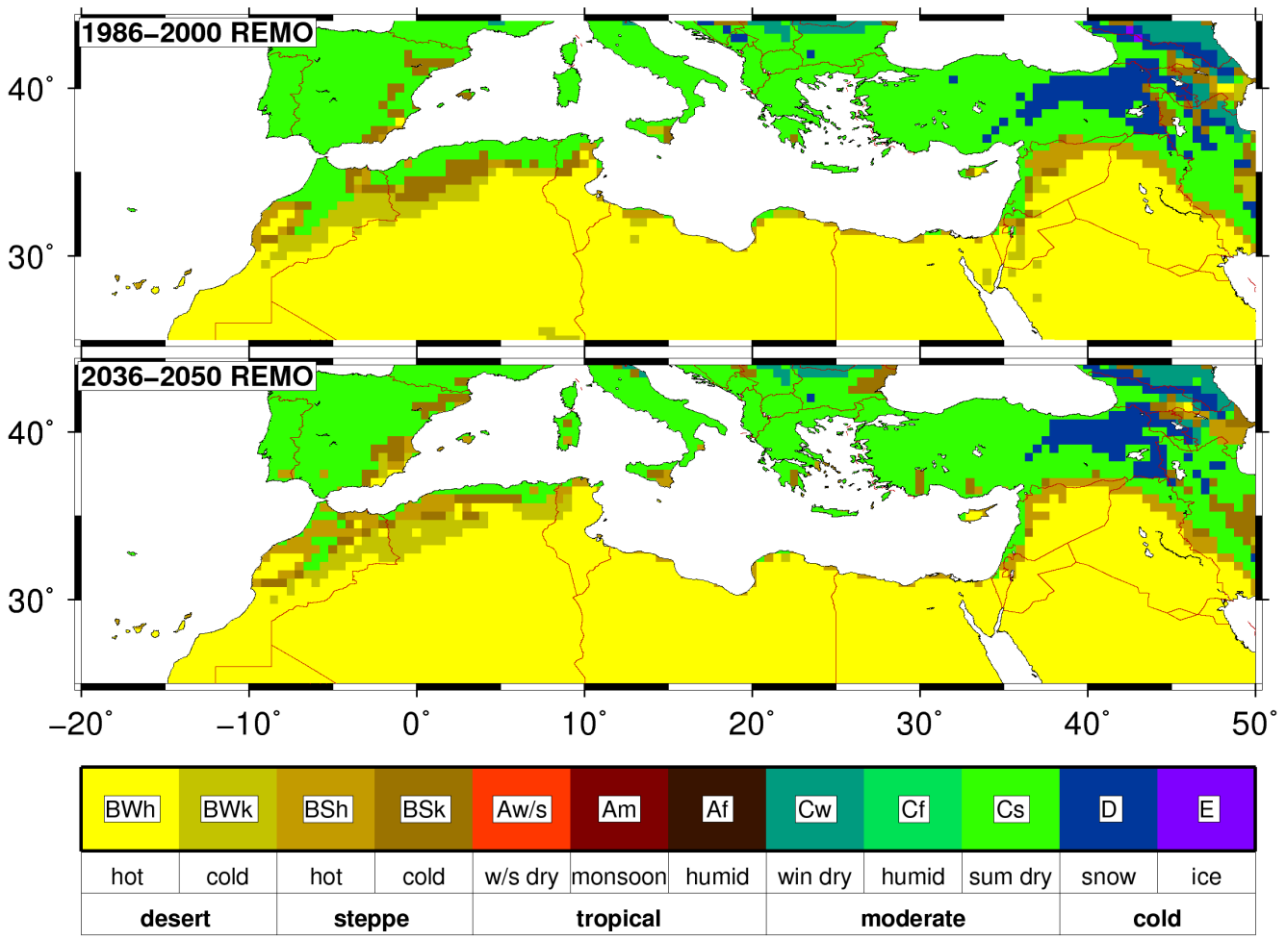

Fig. 3: *Climate classification after Köppen for simulated climate scenarios from REMO.*

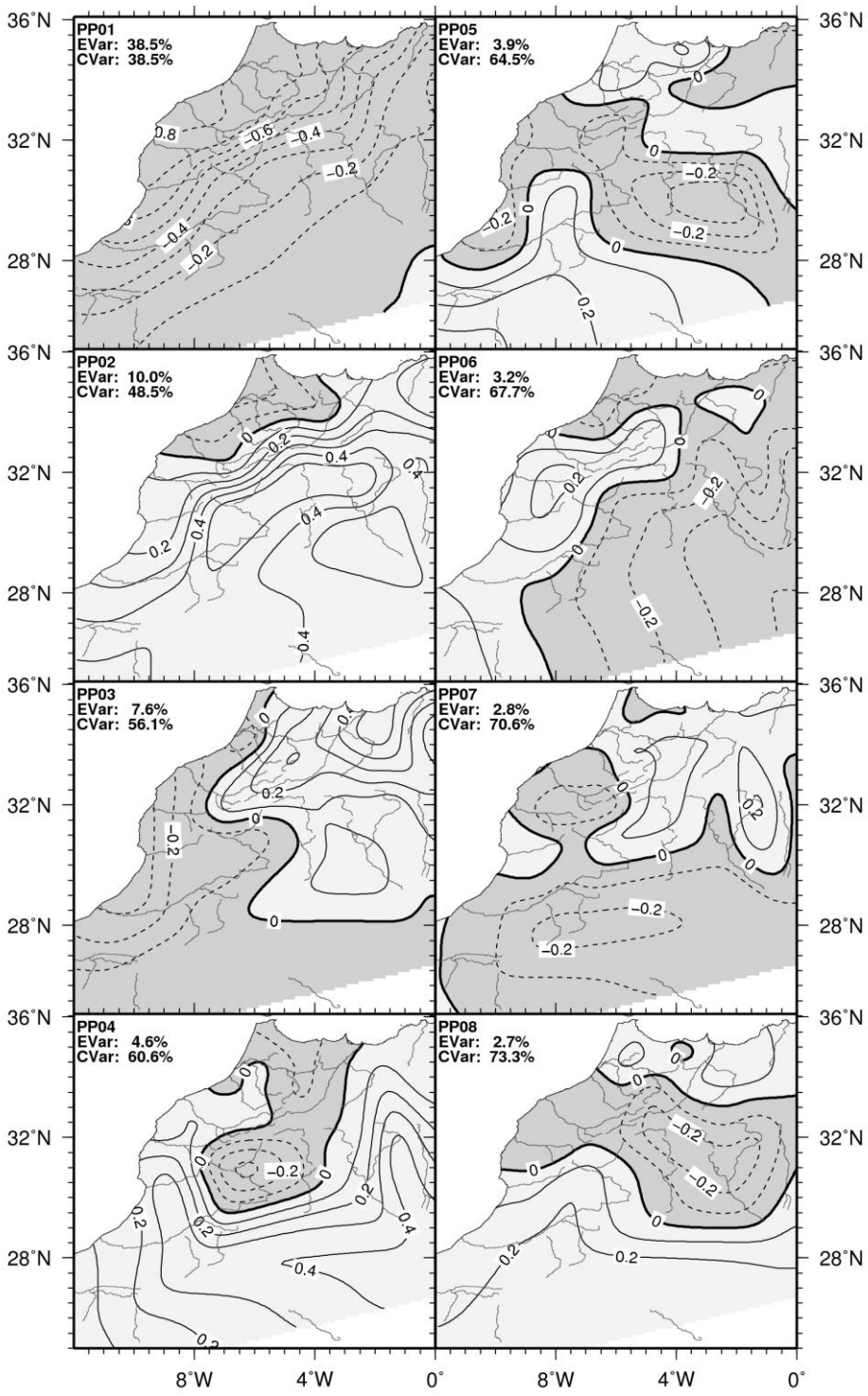

Fig. 4: *The leading eight principal patterns (PP) of the PCA for the period 1951-2000. Continuous contour lines and light grey shading indicate positive, dashed lines and darker grey shading negative values. The numbers in the upper left corners show the explained variance (EV) and the cumulative explained variance (CV) of the first PPs. The PPs are multiplied with the root of the according eigenvalue, so that they represent the correlation patterns. From the first three patterns three characteristic regions are defined: PP01->ATL (Atlantic region), PP02-> SOA (south of the Atlas Mountains) and PP03-> MED (Mediterranean region).*

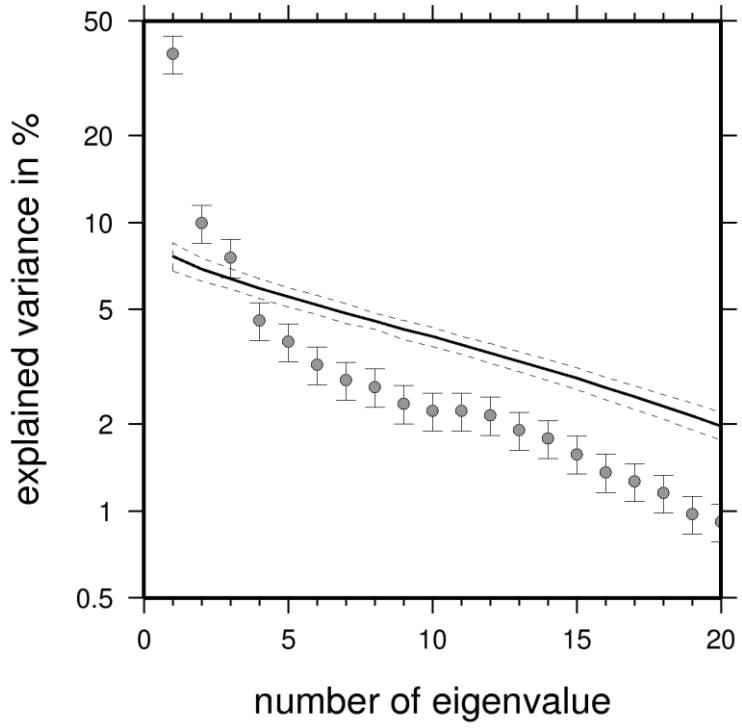

Fig. 5: *Eigenvalues of the PCA (grey circles with error estimates) vs. randomly generated eigenvalues (straight line with broken lines for error estimates). The application of Preisendorfers Rule N shows that only the first three PPs emerge from random noise.*

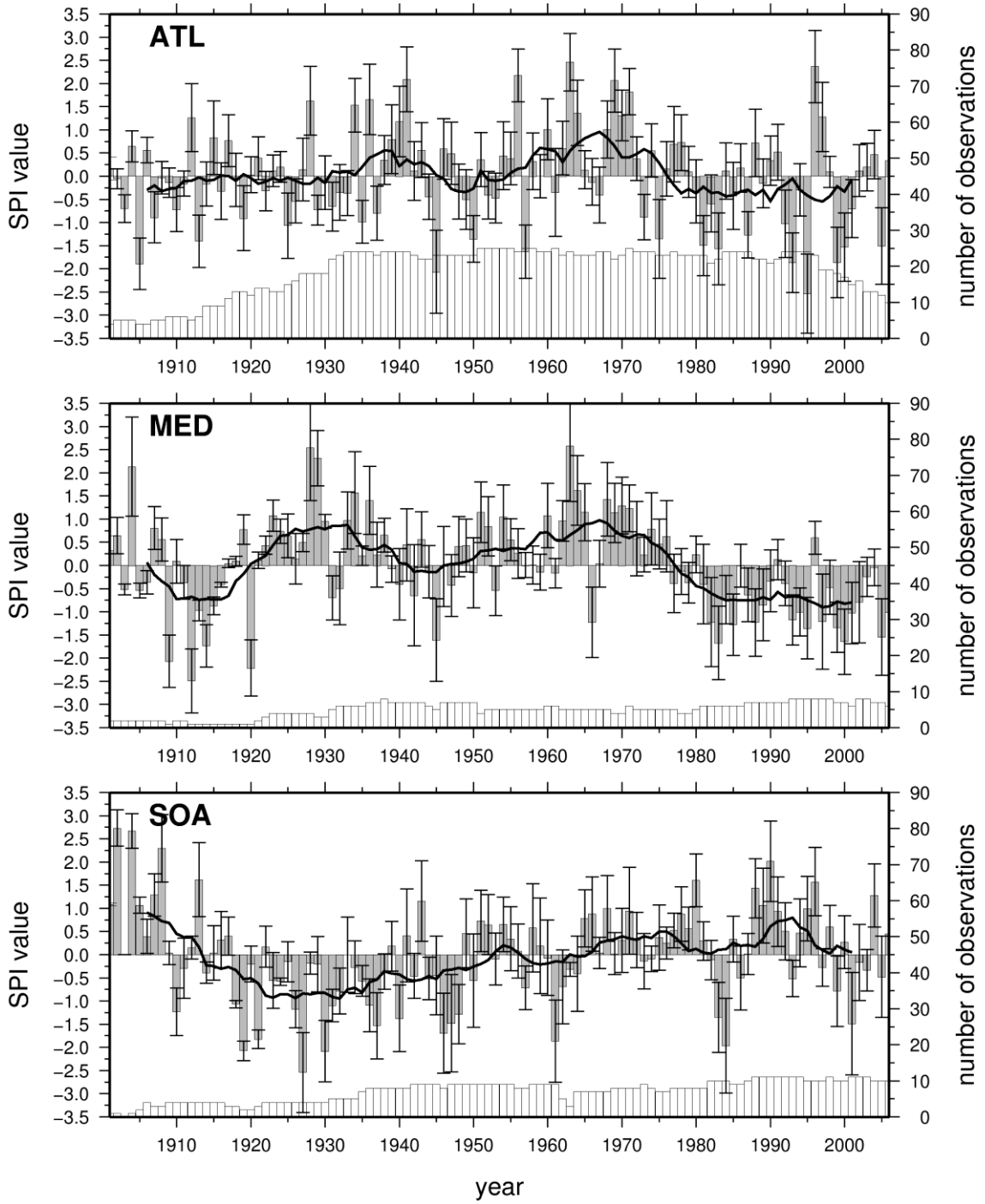

Fig. 6: *Time series of annual SPI values obtained from GHCN station data for the period 1901/2-2006/7 for the Atlantic (ATL), Mediterranean (MED) on southern (SOA) regions. Grey bars: Index values, white bars: number of available stations for each region. As a measure of variability within the regions, the vertical lines centred at the grey bars denote the standard deviation of SPI values of single stations inside each region.*

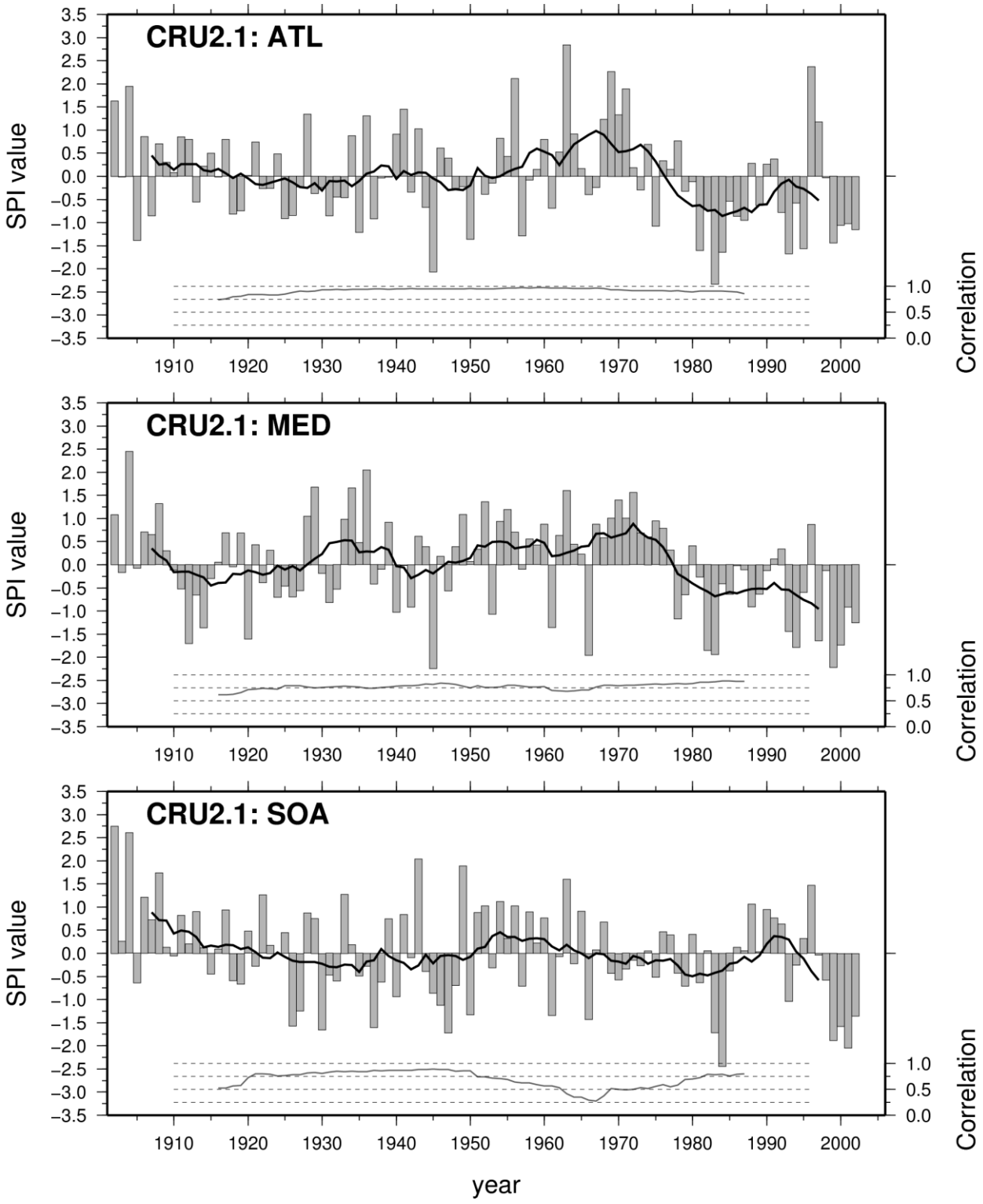

Fig. 7: *Same as Fig. 6, for CRU TS2.1. In the lower part of the panels, time-series of the correlation between SPI values calculated from CRU TS2.1 and GHCN data in a shifting 31-year-window are shown.*

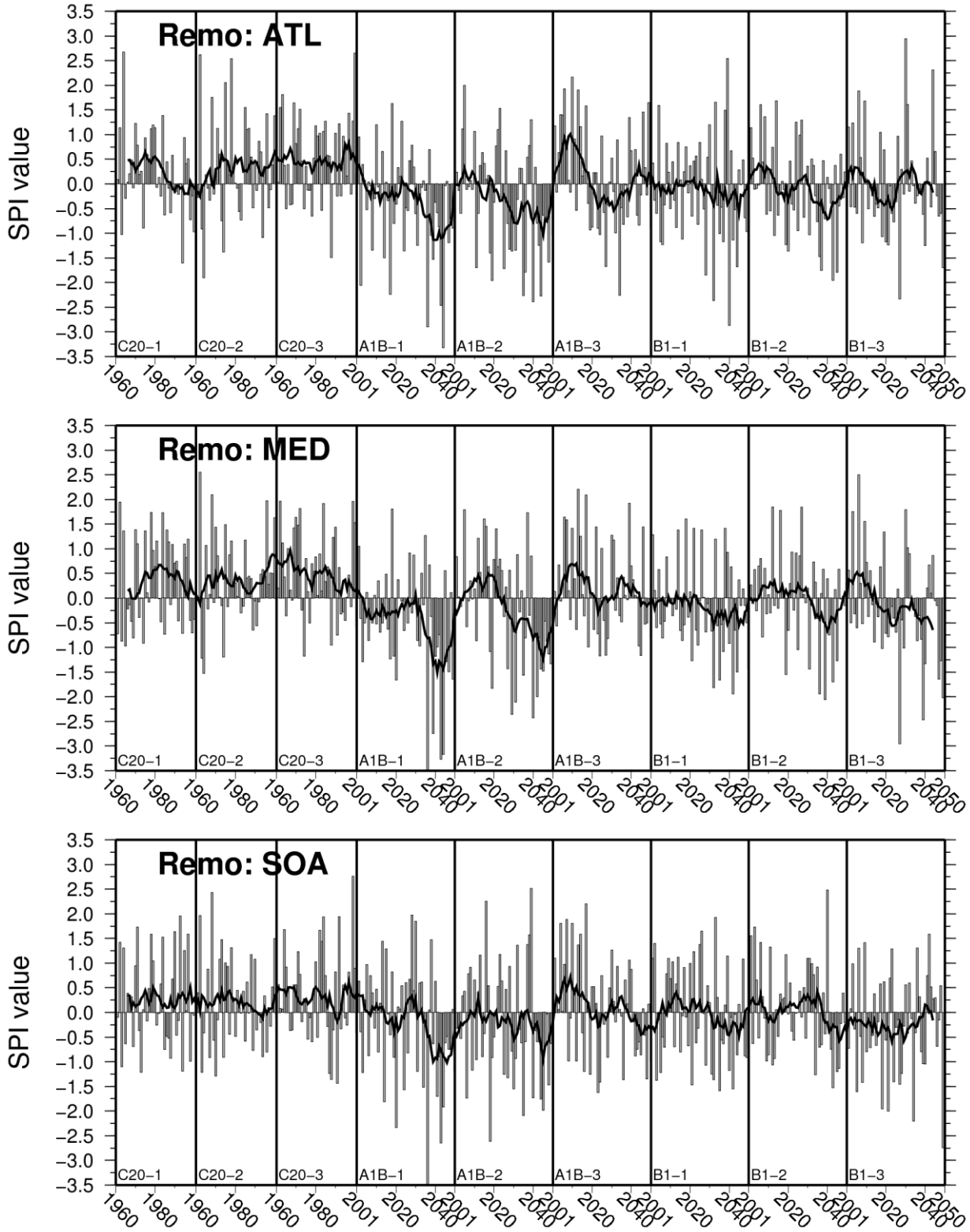

Fig. 8: *Annual SPI values from RCM model runs. In order to enhance the quality of the statistical procedure, all data were collected into one time series of 422 years length. Vertical straight lines mark the intersection between experiments; the labels at bottom axis denote the names of the experiments. C20-1 is the first 1961-2000 experiment, A1B-1 the first scenario SRES A1B experiment and so on. Basis for the SPI calculation was the whole dataset.*

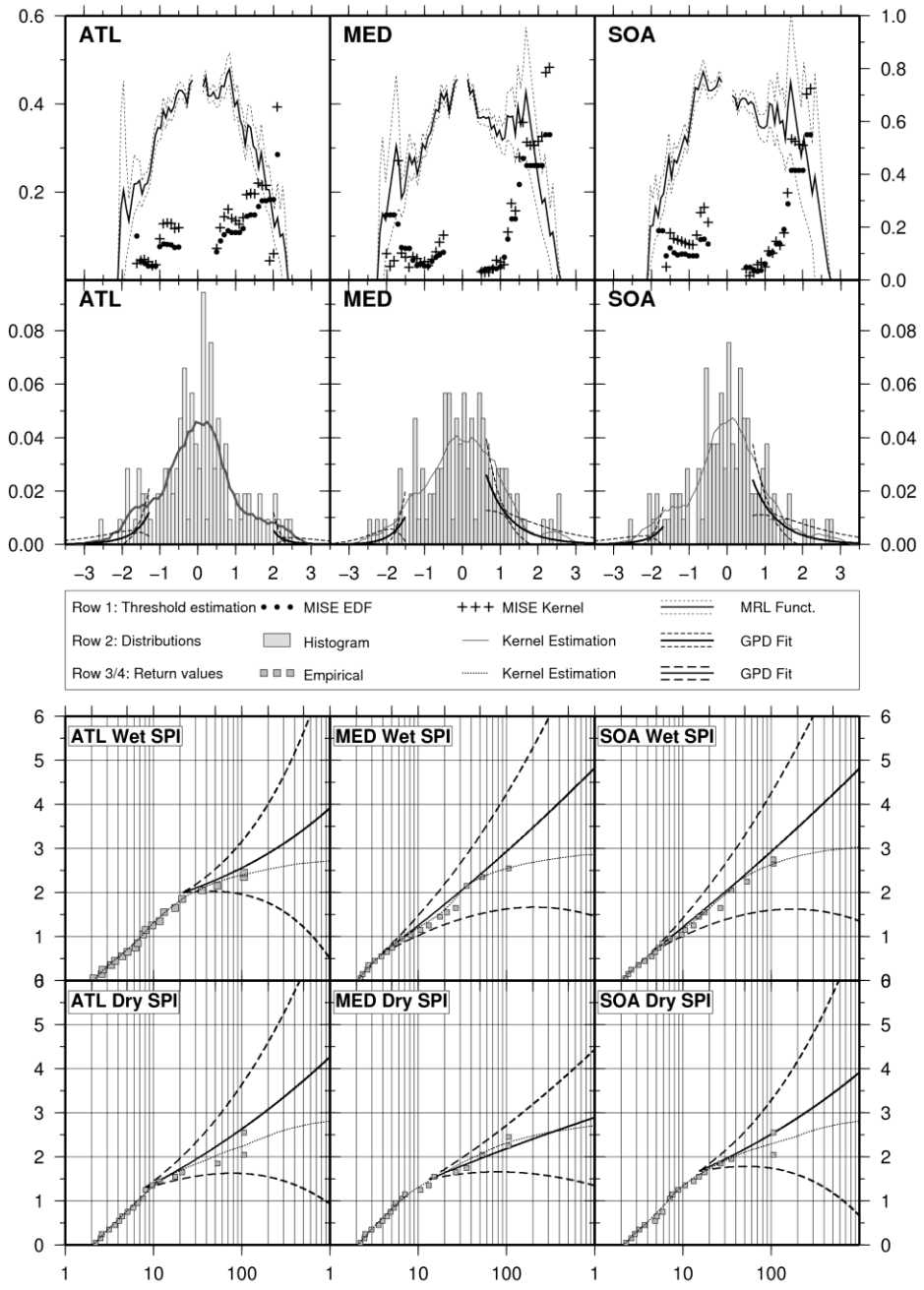

Fig. 9: *Exemplary results of the extreme value analysis for the GHCN data for the period 1901/2-2006/7, for the three regions ATL, MED and SOA.*
Top row: The MRL functions and MISE calculated from EDF and from Gaussian kernel estimation. Vertical axes show on the left side MRL in SPI units, on the right side MISE in SPI units.
Second Row: Distributions, EDF and KDF from SPI data. In addition, the scaled GPD fit to the tails has been added together with the estimated 95% uncertainty. The vertical axis shows probability.
The two bottom rows: Return values obtained from ECD (squares), kernel estimated KCD (broken line) and from GPD analysis (thick lines with broken lines showing the 95% uncertainty range). On the horizontal axes, years are shown, on the vertical SPI units. For the graphics, dry SPI values are changed in sign.

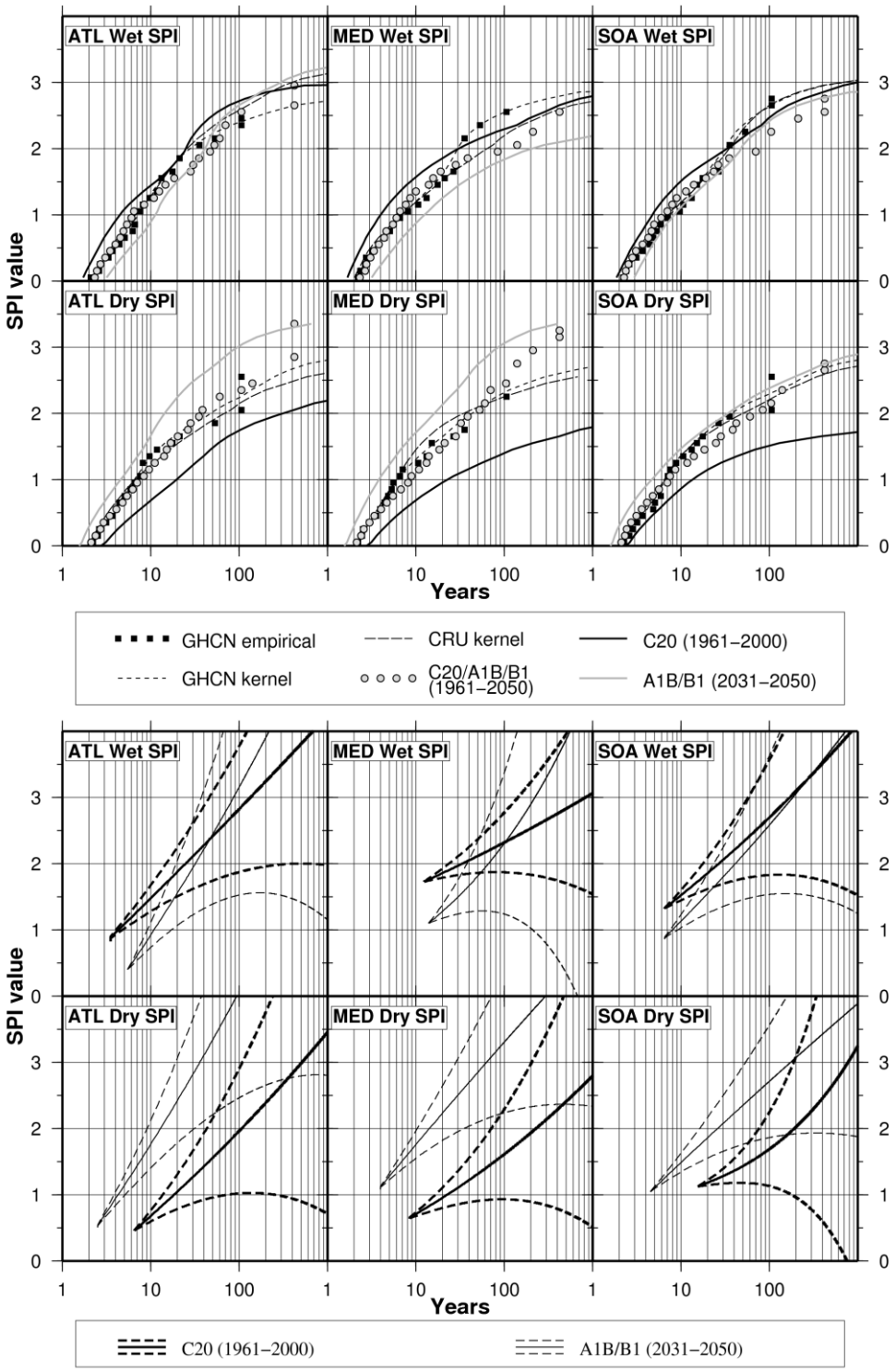

Fig. 10: *Return values of the SPI estimated from RCM compared to values from GHCN observations. For the graphics, the dry SPI values are changed in sign.*
Two upper rows: Wet and dry return values from calculations using empirical and kernel estimated return values on SPI time series. Shown are empirical GHCN observations (1902-2007), kernel estimated GHCN observations (1902-2007), CRU TS2.1, REMO all (1961-2050), REMO C20 (1961-2000) present day climate simulations and REMO A1B and B1 combined scenarios (2031-2050). The two bottom rows show return values obtained from extreme value analysis using the GPD fit, only for REMO C20 and the combined scenarios A1B and B1, again for 2031-2050. The broken lines in the left two columns mark the 95% uncertainty levels.

Table 1: *Definition of classes of the reduced Köppen climate classification. T is the mean monthly temperature in 2m hight above ground, Prec is the annual precipitation sum. Max / Min T indicate the warmest and coldest month in the mean annual cycle.*

Name	Climate	Criterion 1	Criterion 2
E	**Ice**	Max T < 10°C	
D	**Snow**	Max T > 10°C and Min T < -3°C	
Cs	**Moderate**	-3°C < Min T < 18°C	summer dry
Cf			Wet
Cw			winter dry
Af	**Tropical**	Min T > 18°C	Wet
Am			Monsoon climate*
Aw/s			winter/summer dry
BSk	**Steppe**	{Mean T} < {Prec} < 2 {Mean T}	cold (Mean T < 18°C)
BSh			warm (Mean T > 18°C)
BWk	**Desert**	cold with Mean T < 18°C	
BWh		warm with Mean T > 18°C	

* In monsoon climates, the dry period is compensated by annual rainfall: let p_{min} be the rainfall of the driest month, then p_{min} is compensated if Prec > 2500-500*(p_{min} / 20)

Table 2: *Short description of SRES scenario families. The scenarios chosen for future climate scenarios in IMPETUS are shaded.*

		A **Rapid economic growth**	**B** **Environmental sustainable development**	
Global	A1	Globally uniform development: Rapid economic growth, low population growth and rapid introduction of more efficient technologies	B1	As A1, but with rapid changes in economic structures toward a service and information economy, with reductions in material intensity, and the introduction of clean and resource-efficient technologies.
	A1B	As A1, but with a future energy source mix which does not depend on one particular energy source.		
Regional	A2	Regional heterogeneous development: High population growth. Economic development primarily regionally oriented. Economic growth and technological change are more fragmented and slower than in A1.	B2	Emphasis is on **local** solutions to economic, social, and environmental sustainability. Moderate population growth, intermediate economic development, less rapid and more diverse technological change. Focussing on local and regional levels.